RSC Advances

PAPER

View Article Online
View Journal | View Issue

Cite this: *RSC Adv.*, 2017, **7**, 46499

Instantaneous preparation of high lithium-ion conducting sulfide solid electrolyte $Li_7P_3S_{11}$ by a liquid phase process

Marcela Calpa,[a] Nataly Carolina Rosero-Navarro,*[b] Akira Miura[b] and Kiyoharu Tadanaga[b]

Received 17th August 2017
Accepted 26th September 2017

DOI: 10.1039/c7ra09081a

rsc.li/rsc-advances

A solid electrolyte with a small particle size, good mechanical properties and high ionic conductivity is required to achieve high energy and power density in the all-solid-state battery. Here, we report an instantaneous preparation of high lithium-ion conducting sulfide solid electrolyte $Li_7P_3S_{11}$ by a simple procedure involving a liquid phase process under ultrasonic irradiation and low thermal treatment at 220 °C. A short reaction time of 30 min was enough to produce the formation of PS_4^{3-} units. Subsequent drying and heating processes led to the precipitation of the $Li_7P_3S_{11}$ phase with a particle size below 500 nm, achieving high ionic conductivity of 1.0×10^{-3} S cm^{-1} at 22 °C and a low activation energy of 12.8 kJ mol^{-1}.

1. Introduction

The development of large-scale power storage systems with high energy density has become essential to advance renewable energy and electric vehicles. This trend has led to an increasing demand for lithium ion secondary batteries as they are considered to offer the high energy density required. However, lithium ion batteries using organic liquid electrolytes can carry safety issues because of the risk of leakage and flammability. All-solid-state lithium ion secondary batteries using inorganic solid electrolytes have been studied in the last two decades as the next-generation batteries, because of their higher safety. Moreover, the solid electrolytes[1–3] have a wider electrochemical window making them compatible with high voltage cathodes, therefore higher energy densities can be achieved.

Oxide and sulfide solid electrolytes with conductivities comparable to those of liquid electrolytes have been reported, although sulfide electrolytes have a rather higher conductivity than oxide electrolytes, around 10^{-2} S cm^{-1}.[1,4] Also, sulfide-based solid electrolytes are one of the most promising solid electrolytes for all-solid-state batteries, not only because their high ionic conductivity, but also because their good mechanical properties, that allows an intimate contact in the interface between electrode and electrolyte by using only room temperature pressing.[5] A good ionic conduction path at the solid–solid interface between electrode active material and solid electrolyte is a key factor for improving the cycle performance of the all-solid-state battery.[6–9] Thus, the morphology of the sulfide solid electrolyte is also important. Small sized particles with a large interfacial area entail a dense and homogenous electrolyte and electrode composite, which increases the energy density of the all-solid-state battery.[8–10] Sulfide-based solid electrolytes generally are synthesized by the ball milling method,[11] which requires high synthesis energy and a long-time, more than 24 h. Recently, liquid phase synthesis using an organic solvent has been reported. Smaller particle size, in the nanometer range, has been obtained by this process.[2,12–14] The synthesis of Li_3PS_4 has been mediated by different organic solvents such as *n*-methylformamide[15] acetonitrile,[16] tetrahydrofuran[2] and ethyl acetate,[17] and conductivities around 10^{-4} and 10^{-6} S cm^{-1} have been obtained. The reaction process involves more than 24 h of magnetic stirring, and subsequent heat treatment to obtain stable Li_3PS_4. Reduction of the time during reaction process has been attained by synthesis *via* liquid-phase shaking, using zirconia balls, and ethyl propionate[18] or dimethyl carbonate[13] as solvent. In this case, 6 hours for the reaction process was required.

On the other hand, the synthesis of $Li_7P_3S_{11}$ crystal phase by liquid phase process, has been mediated by solvents such as 1,2-dimethoxyethane,[12] acetonitrile[14,19] and tetrahydrofuran.[19] Higher ionic conductivities of the order of 10^{-3} and 10^{-4} S cm^{-1} have been obtained, but reaction times from 24 h[14,19] to more than 3 days were required. To date, no deep investigation about the necessary time for the reaction process has been reported. A new process that entails a short time for the reaction, while ensuring sufficiently high ionic conductivity and small particle size is desirable.

Solvent interaction during liquid phase synthesis is fundamental in the morphology of the sulfide solid electrolyte.

[a]*Graduate School of Chemical Sciences and Engineering, Hokkaido University, Sapporo, Japan*

[b]*Division of Applied Chemistry, Faculty of Engineering, Hokkaido University, Sapporo 060-8628, Japan. E-mail: rosero@eng.hokudai.ac.jp*

Acetonitrile is a good candidate as solvent as it has a low vapor pressure (13.3 kPa at 25 °C) and allows the growth of smaller individual particles of around 2 μm,[16] compared for instance with the tetrahydrofuran solvent that leads to obtaining larger particles of around 10 μm.[2,16]

In addition, ultrasonic irradiation is a useful technique to enhance chemical reactivity in a solid–liquid system. The implosion of cavitation bubbles during ultrasonication generate local high temperatures and pressures, and this large amount of energy stimulates chemical activity.[20,21]

Herein we report for the first time an instantaneous preparation of high lithium-ion conducting sulfide solid electrolyte $Li_7P_3S_{11}$ by a simple procedure involving a liquid phase process and ultrasonic irradiation.

2. Experimental section

Synthesis

Li_2S (Mitsuwa Chemical, 99.9%) and P_2S_5 (Aldrich, 99%) with a stoichiometry of 74 to 26 were mixed in anhydrous acetonitrile (Wako Pure Chemical Industries). The mixture was ultrasonicated at 60 °C for 30 min under 28 kHz using an ultrasonic bath (Shimadzu SUS-103). The ultrasonication process formed a white suspension (named as SSE-slurry). Consequent drying process was applied at 180 °C for 3 h under vacuum to remove the solvent and obtain solid powders (named as SSE-180). Subsequently, heat treatment at 220 °C for 1 h was carried out to promote the crystallization of the $Li_7P_3S_{11}$ sulfide electrolyte. The crystallized powder hereafter is named as SSE-220. Fig. 1 shows photographs taken during the synthesis procedure illustrating the material state in each synthesis step.

Characterization

Crystal phase and chemical composition of the sulfide based materials were studied by X-ray diffraction (XRD) and Raman spectroscopy. XRD measurements were performed using a CuKα radiation with an X-ray diffractometer (Miniflex 600, Rigaku) to identify crystalline phase of the samples. Diffraction data were collected in 0.01° steps from 10° to 40° in 2θ.

Raman spectroscopy was performed using a Raman spectrometer (HORIBA XploRA PLUS Scientific) to identify structural units of the samples. Raman shift was ranged between 300 cm^{-1} and 3050 cm^{-1}. Morphology of the sulfide solid electrolyte particles was observed by scanning electron microscopy (SEM), performed on a JIB-4600F Multibeam SEM-FIB Scanning Electron Microscope.

The ionic conductivity of pelletized samples was evaluated by electrochemical impedance spectroscopy (EIS). The solid electrolyte powders (Approximately 80 mg) were pressed under 360 MPa (at room temperature) in a polycarbonate tube with 10 mm of diameter, two stainless steel (SS) disks were used as current collectors. EIS measurements were conducted using an impedance analyser (SI 1260, Solartron) in the frequency range of 0.1 MHz to 1 Hz at the amplitude of 30 mV. The spectra were analysed with the ZView software (Version 3.3f, Scribner Associates) in order to assess the ohmic resistance (R) of the pellet. For the activation energy measurement, the temperature was controlled from −50 °C to 60 °C.

Electrochemical properties of the SSE-220 sample were evaluated by a cyclic voltammetry technique. The solid electrolyte powders (approximately 140 mg) were pelletized at 360 MPa. A cell of Li/SSE-220/SS was constructed by carefully attaching Li to one of the current collectors. The cyclic voltammogram measurement was conducted using a potentiostat/galvanostat device (SI 1287, Solartron) in the potential range of −0.5 V to 5 V (*vs.* Li/Li^+) at a scanning rate of 1 mV s^{-1}. All processes were performed in an argon atmosphere.

3. Results and discussion

Fig. 2 shows the XRD patterns of the SSE-180 and SSE-220 samples. The indexed diffraction pattern of the $Li_7P_3S_{11}$ phase (ICDD#157564, Fig. 2c) is shown for comparison. A complex

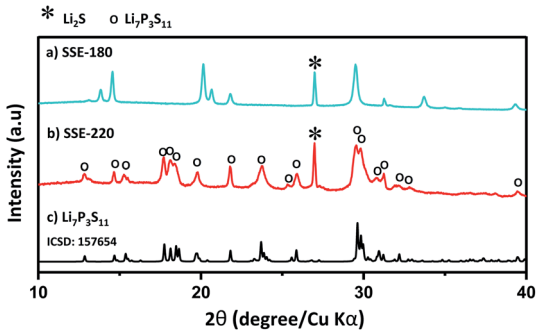

Fig. 2 XRD patterns of the: (a) SSE-180 and (b) SSE-220 samples. (c) XRD pattern of $Li_7P_3S_{11}$ phase (ICDD#157564).

Fig. 1 Photographs of material state during the synthesis procedure.

pattern with undefined peaks was obtained after the drying process at 180 °C (Fig. 2a). The peak corresponding to the Li_2S phase precursor is identified, but the other peaks were not able to be associated to P_2S_5 precursor or any solid electrolyte phases. Peaks corresponding to $Li_7P_3S_{11}$ phase were observed only after heat treatment at 220 °C (Fig. 2b). The presence of Li_2S phase was also identified.

The structural units of the solid electrolyte during the synthesis process was also examined by using Raman spectroscopy. Fig. 3 shows the Raman spectra of the SSE-slurry, SSE-180 and SSE-220 samples. A main band at 428 cm^{-1}, attributed to the PS_4^{3-} (*ortho*-thiophosphate) units,[22] was observed after 30 min of ultrasonic irradiation (SSE-slurry sample). Bands located around 370 cm^{-1}, 900 cm^{-1}, 2200 cm^{-1} and 2900 cm^{-1}, corresponding to C–C≡N bending, C–C stretch, C≡N stretching and symmetric C–H stretch vibrations of acetonitrile[23,24] were identified. After drying at 180 °C, similar bands were also observed, revealing that the powder is composed mainly by PS_4^{3-} units and the remained acetonitrile.

The Raman spectra of the as-synthesized powder after heat treatment at 220 °C shows only a main wide band at 405 cm^{-1}, attributed to $P_2S_7^{4-}$ (*pyro*-thiophosphate) units.[22] The bands associated to acetonitrile completely disappeared, confirming the full removal of the solvent. The heat treatment at 220 °C, to remove the remaining solvent, promoted also a structure rearrangement of PS_4^{3-} units into $P_2S_7^{4-}$ units. The studies of the crystal $Li_7P_3S_{11}$ structure suggest that this contains mainly $P_2S_7^{4-}$ ditetrahedral and PS_4^{3-} tetrahedral units.[25] Fig. 3c shows the deconvolution of the band of the as-synthesized powder after heat treatment at 220 °C using a Gaussian–Lorentzian function. Two bands centered at 420 cm^{-1} and 404 cm^{-1} confirmed the presence of $P_2S_7^{4-}$ and PS_4^{3-} units,[22,26] respectively. A third band centered at 385 cm^{-1} was also found and is associated to $P_2S_6^{4-}$ unit. The major fraction, corresponds to $P_2S_7^{4-}$ and PS_4^{3-} units. A small concentration of $P_2S_6^{4-}$ unit has also been identified in the high ionic conductor $Li_7P_3S_{11}$ obtained by mechanical milling. Higher contents of $P_2S_6^{4-}$ unit could lead to the dramatical drop of the ionic conduction.[27,28]

The results of Raman spectra are in good agreement with the results obtained by X-ray diffraction (Fig. 2). According to Raman spectra, the unknown peaks observed in the XRD pattern of the powder dried at 180 °C (Fig. 2a), are ascribed to the formation of complexes between PS_4^{3-} units and remained acetonitrile.[14] The main $Li_7P_3S_{11}$ crystal phase observed after heat treatment at 220 °C is composed by $P_2S_7^{4-}$, PS_4^{3-} and $P_2S_6^{4-}$ units, confirmed by the Raman spectra analysis.

The additional intense peak associated to Li_2S phase, observed after drying process at 180 °C and heat treatment at 220 °C, can be explained by the possible formation mechanism of the $Li_7P_3S_{11}$ crystal phase. It is believed, that the rearrangement of the structure produced during the heat treatment at 220 °C led to the formation of Li_2S as a sub-product of this reaction.

Fig. 4 shows the morphology of the SSE-180 and SSE-220 samples. After drying at 180 °C, big agglomerates (approx. 5–20 μm) and irregular particles with a small particle size around 500 nm were observed. After heat treatment at 220 °C, the particle size was irregular, but remains in the nanometric range. Inset in Fig. 4b shows smaller individual particles lower than 500 nm. The small particle size is attributed to the interaction between solvent and particles during the synthesis process. Acetonitrile can play a surfactant function,[16] leading to obtain a better dispersion of the powder during the ultrasonication and further a good control of the particle size growth during the solvent removal. In contrast, preparation of sulfide solid electrolyte by ball milling produces particle sizes greater than 10 μm.[10] A smaller particle size should improve the contact at the solid–solid interface between active material and solid electrolyte, which is a key factor to obtaining a good performance in the all-solid-state battery.[10]

Fig. 5a shows the impedance spectra of the pelletized SSE-180 and SSE-220 samples, correspondingly. The impedance spectra of the SSE-180 sample consists of a well-defined semicircle at high frequency due to bulk and grain boundary resistances and a capacitive tail at low frequency due to the electrodes interface. The data was fitted with a simple

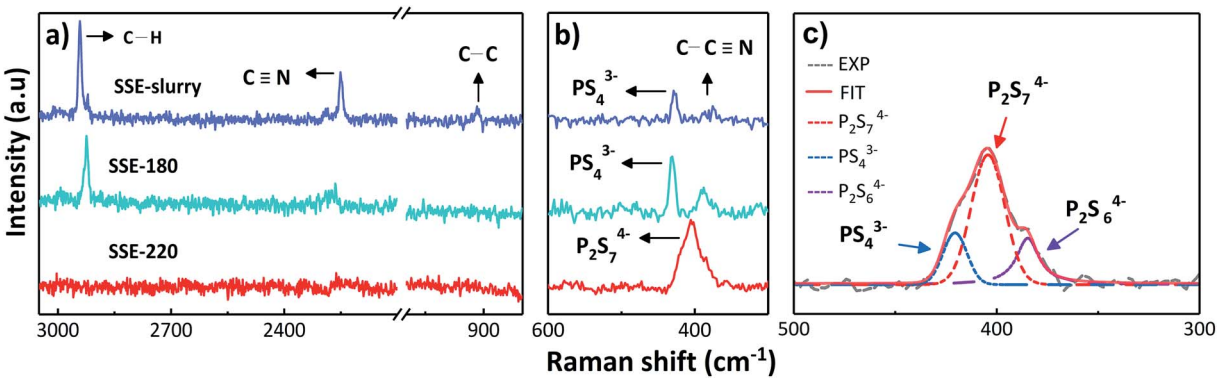

Fig. 3 Raman spectra of the $74Li_2S{\cdot}26P_2S_5$ sulfide electrolyte in the range of (a) 3050–850 cm^{-1} and (b) 600–300 cm^{-1}. Blue, green and red lines represent SSE-slurry, SSE-180 and SSE-220 samples, correspondingly. (c) Spectral decomposition of Raman spectrum for the SSE-220 sample. Dashed grey line, experimental data; continuous orange line, the fitting result for all PSx polyhedral; dashed red, blue and violet lines, $P_2S_7^{4-}$, PS_4^{3-} and $P_2S_6^{4-}$ units, correspondingly.

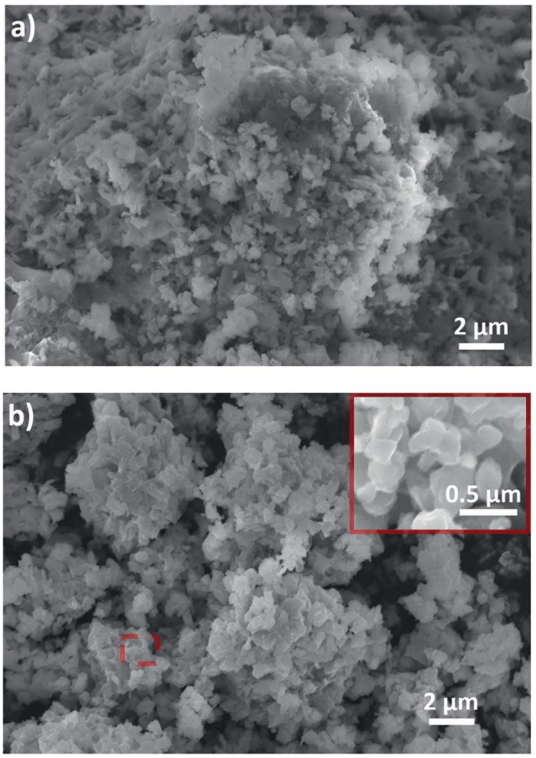

Fig. 4 Micrographs of the (a) SSE-180 and (b) SSE-220 samples.

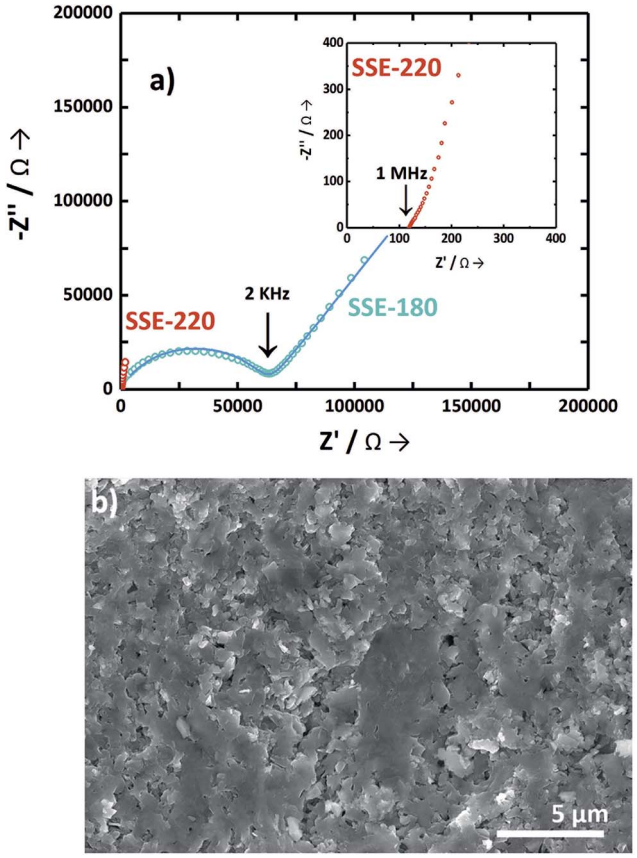

Fig. 5 (a) Impedance spectra of the pelletized SSE-180 (dotted green line: EIS data, continuous blue line: fitted data) and SSE-220 (dotted red line) samples. (b) Cross-section micrograph of the SSE-220 sample.

equivalent circuit comprising a resistor in parallel with a capacitor ($R\|C$, C is a constant phase element) to describe the pellet electrical behavior. In addition, a capacitor in series was used to simulate the contribution of the electrodes interface. The fitting results was drawn together with the EIS data. The total resistance (bulk and grain boundary resistances), was used to calculate the ionic conductivity, attaining 1.4×10^{-6} S cm^{-1} (22 °C). The impedance spectra of the SSE-220 sample does not exhibit the full semicircle due to the lower resistance. In this case, the resistance was estimated by the value of Z' at the intercept with the real axis obtained by linear fitting. The ionic conductivity of the SSE-220 sample attained 1.0×10^{-3} S cm^{-1} (22 °C).

Fig. 5b shows the cross-section micrograph of the SSE-220 pellet. Cross-section micrograph displays a compact surface with a tight contact of micronized particles. There is almost no crack, but microporous were observed.

Total ionic conductivity can be increased by reducing the grain boundary resistance through pellet densification.[4] Densities in the range of 1.45 g cm^{-3} and 1.53 g cm^{-3} were achieved by applying cold pressure between 350 MPa and 500 MPa to the SSE-220 sample. In dependency of the obtained densities, the ionic conductivity range between 0.9×10^{-3} S cm^{-1} and 1.5×10^{-3} S cm^{-1} at 22 °C.

In accordance with the XRD and Raman studies, the low ionic conductivity of the SSE-180 sample was expected, due to the insufficient acetonitrile removal. Further, the rather low temperature of 220 °C was efficient enough to remove acetonitrile, as well as to promote the crystallization of the $Li_7P_3S_{11}$ phase with a consequent high conductivity. In addition, the small particle obtained in the nanometric range allowed a good densification to be obtained by a simple cold pressure. The high ionic conductivity of the $Li_7P_3S_{11}$ (SSE-220) reported in this work is comparable to the $Li_7P_3S_{11}$ solid electrolyte obtained by mechanical milling (3.2×10^{-3} S cm^{-1} at RT, 30 h of synthesis process)[11] or by liquid phase (1.5×10^{-3} S cm^{-1} at 25 °C, 37 h of synthesis process).[14]

Fig. 6 shows the temperature dependency of the ionic conductivity of the SSE-220 sample. A low activation energy of 12.8 kJ mol^{-1} was calculated. In comparison, $Li_7P_3S_{11}$ solid electrolyte is reported to have an activation energy of 12 kJ mol^{-1} when the synthesis is carried out by mechanical milling[11] and 23 kJ mol^{-1} when the synthesis is carried out by liquid phase.[14] The lower activation energy reported here, in comparison with other $Li_7P_3S_{11}$ solid electrolyte obtained by a liquid phase process, is assumed to be because of the higher crystallization degree,[11] as well as good densification by the smaller particle size. The synthesis described in this work allows an effective synergy between the control of the crystal structure and particle size to attain high ionic conduction and lower activation energy.

Fig. 7 shows the cyclic voltammogram of the SSE-220 sample, from −0.5 V to 5 V (*vs.* Li/Li$^+$). Both cathodic and anodic current peaks assigned to the lithium deposition ($Li^+ + e^- \rightarrow Li$) and

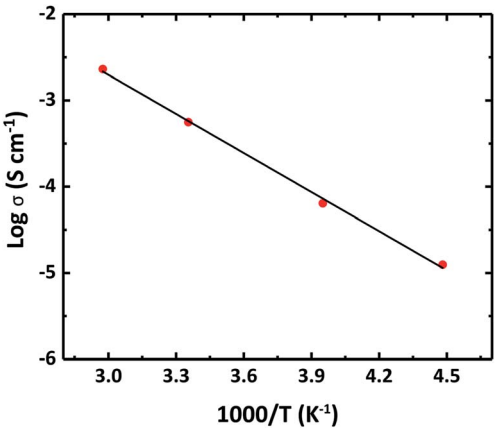

Fig. 6 Temperature dependency of the ionic conductivity of SSE-220 sample.

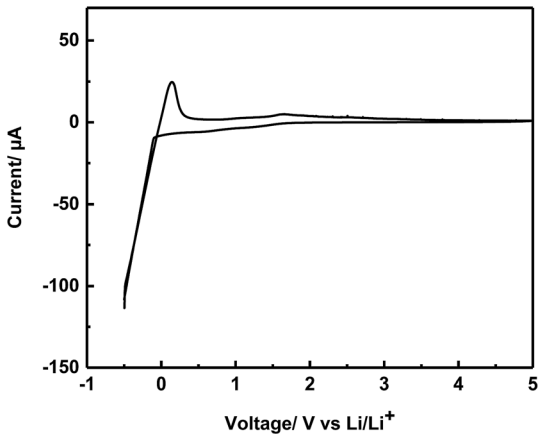

Fig. 7 Cyclic voltammogram of the SSE-220 sample using a cell constructed of Li/SSE-220/SS, in the potential range from −0.5 V to 5 V (*vs.* Li/Li^+) at a scanning rate of 1 mV s^{-1}.

dissolution ($Li \rightarrow Li^+ + e^-$) reactions were observed in the potential range of −0.5 V to 0.5 V in the voltammogram, suggesting that the synthesized solid electrolyte is electrochemically stable for lithium metal. A small anodic current peak was observed around 2 V, this is probably attributed to the oxidation of free S^{2-} ions as a similar behavior was observed in the cyclic voltammogram of the solid electrolyte $Li_7P_3S_{11}$ synthesized by mechanical milling.[28] These results indicate that the synthesized $Li_7P_3S_{11}$ solid electrolyte (SSE-220) has a wide and electrochemical window up to 5 V (*vs.* Li/Li^+).

4. Conclusion

The high lithium-ion conducting sulfide solid electrolyte $Li_7P_3S_{11}$ has been successfully synthesized by an instantaneous preparation involving a liquid phase process under ultrasonic irradiation followed by drying and low thermal treatment. Interaction between solvent and Li_2S and P_2S_5 precursors particles during ultrasonication and further removal of the solvent at rather low temperatures of 220 °C led to obtain smaller particle size lower than 500 nm, less than 10 times to the particle size of the solid electrolyte typically obtained by mechanical milling. The high ionic conductivity of 1.0×10^{-3} and the low activation energy of 12.8 kJ mol^{-1} was achieved because of the good crystallization of the $Li_7P_3S_{11}$ phase.

Conflicts of interest

There are no conflicts to declare.

Acknowledgements

The present work was supported by the Japan Science and Technology Agency (JST), Advanced Low Carbon Technology Research and Development Program (ALCA), and Specially Promoted Research for Innovative Next Generation Batteries (SPRING) project. The analysis of SEM was carried out with JIB-4600F at the "Joint-use Facilities: Laboratory of Nano-Micro Material Analysis", Hokkaido University, supported by "Material Analysis and Structure Analysis Open Unit (MASAOU)".

References

1 N. Kamaya, K. Homma, Y. Yamakawa, M. Hirayama, R. Kanno, M. Yonemura, T. Kamiyama, Y. Kato, S. Hama, K. Kawamoto and A. Mitsui, *Nat. Mater.*, 2011, **10**, 682–686.
2 Z. C. Liu, W. J. Fu, E. A. Payzant, X. Yu, Z. L. Wu, N. J. Dudney, J. Kiggans, K. L. Hong, A. J. Rondinone and C. D. Liang, *J. Am. Chem. Soc.*, 2013, **135**, 975–978.
3 J. C. Li, C. Ma, M. F. Chi, C. D. Liang and N. J. Dudney, *Adv. Energy Mater.*, 2015, **5**, 1–6.
4 Y. Seino, T. Ota, K. Takada, A. Hayashi and M. Tatsumisago, *Energy Environ. Sci.*, 2014, **7**, 627–631.
5 A. Sakuda, A. Hayashi and M. Tatsumisago, *Sci. Rep.*, 2013, **3**, 1–5.
6 M. Nagao, A. Hayashi and M. Tatsumisago, *Electrochim. Acta*, 2011, **56**, 6055–6059.
7 T. Minami, A. Hayashi and M. Tatsumisago, *Solid State Ionics*, 2006, **177**, 2715–2720.
8 A. Sakuda, A. Hayashi, T. Ohtomo, S. Hama and M. Tatsumisago, *J. Power Sources*, 2011, **196**, 6735–6741.
9 N. C. Rosero-Navarro, T. Kinoshita, A. Miura, M. Higuchi and K. Tadanaga, *Ionics*, 2017, **23**, 1619–1624.
10 A. Sakuda, T. Takeuchi and H. Kobayashi, *Solid State Ionics*, 2016, **285**, 112–117.
11 F. Mizuno, A. Hayashi, K. Tadanaga and M. Tatsumisago, *Solid State Ionics*, 2006, **177**, 2721–2725.
12 S. Ito, M. Nakakita, Y. Aihara, T. Uehara and N. Machida, *J. Power Sources*, 2014, **271**, 342–345.
13 N. H. H. Phuc, K. Morikawa, M. Totani, H. Muto and A. Matsuda, *Solid State Ionics*, 2016, **285**, 2–5.
14 X. Y. Yao, D. Liu, C. S. Wang, P. Long, G. Peng, Y. S. Hu, H. Li, L. Q. Chen and X. X. Xu, *Nano Lett.*, 2016, **16**, 7148–7154.
15 S. Teragawa, K. Aso, K. Tadanaga, A. Hayashi and M. Tatsumisago, *J. Mater. Chem. A*, 2014, **2**, 5095–5099.
16 H. Wang, Z. D. Hood, Y. N. Xia and C. D. Liang, *J. Mater. Chem. A*, 2016, **4**, 8091–8096.

17 N. H. H. Phuc, M. Totani, K. Morikawa, H. Muto and A. Matsuda, *Solid State Ionics*, 2016, **288**, 240–243.
18 N. H. H. Phuc, K. Morikawa, T. Mitsuhiro, H. Muto and A. Matsuda, *Ionics*, 2017, 1–7.
19 R. C. Xu, X. H. Xia, Z. J. Yao, X. L. Wang, C. D. Gu and J. P. Tu, *Electrochim. Acta*, 2016, **219**, 235–240.
20 K. S. Suslick, *Sci. Am.*, 1989, **260**, 80–86.
21 S. Chida, A. Miura, N. C. Rosero-Navarro, M. Higuchi, N. H. H. Phuc, H. Muto, A. Matsuda and K. Tadanaga, 2017, submitted.
22 M. Tachez, J.-P. Malugani, R. Mercier and G. Robert, *Solid State Ionics*, 1984, **14**, 181–185.
23 C. Chen, X. Huang, D. Lu, Y. Huang, B. Han, Q. Zhou, F. Li and T. Cui, *RSC Adv.*, 2015, **5**, 84216–84222.
24 J. C. Deàk, L. K. Iwaki and D. D. Dlott, *J. Phys. Chem. A*, 1998, **102**, 8193–8201.
25 H. Yamane, M. Shibata, Y. Shimane, T. Junke, Y. Seino, S. Adams, K. Minami, A. Hayashi and M. Tatsumisago, *Solid State Ionics*, 2007, **178**, 1163–1167.
26 F. Mizuno, A. Hayashi, K. Tadanaga and M. Tatsumisago, *Adv. Mater.*, 2005, **17**, 918–921.
27 K. Ohara, A. Mitsui, M. Mori, Y. Onodera, S. Shiotani, Y. Koyama, Y. Orikasa, M. Murakami, K. Shimoda and K. Mori, *Sci. Rep.*, 2016, **6**, 1–9.
28 A. Hayashi, K. Minami and M. Tatsumisago, *J. Solid State Electrochem.*, 2010, **14**, 1761–1767.